

Unlabeled Samples Generated by GAN Improve the Person Re-identification Baseline *in vitro*

Zhedong Zheng, Liang Zheng and Yi Yang

University of Technology Sydney

zdzheng12, liangzheng06, yee.i.yang@gmail.com

Abstract

In this paper, we mainly contribute a simple semi-supervised pipeline which only uses the original training set without extra data collection. It is challenging in 1) how to obtain more training data only from the training set and 2) how to use the newly generated data. In this work, the generative adversarial networks (GANs) are used to generate unlabeled samples. We propose the label smoothing regularization for outliers (LSRO) scheme. It assigns a uniform label distribution to the unlabeled images, which regularizes the supervised model and improves a ResNet baseline.

We verify the proposed method on a practical task: person re-identification (re-ID). This task aims to retrieve the query person from other cameras. We adopt DCGAN [23] for sample generation, and a baseline convolutional neural network (CNN) for embedding learning. In our experiment, we show that adding the GAN-generated data effectively improves the discriminative ability of the learned feature embedding. We evaluate the re-ID performance on two large-scale datasets: Market1501 [45] and CUHK03 [18]. We obtain +4.37% and +1.6% improvement in rank-1 precision over the CNN baseline on Market1501 and CUHK03, respectively.

1. Introduction

Unsupervised learning can serve as an important auxiliary task to supervised tasks [12, 25, 9, 24]. In this work, we propose a semi-supervised pipeline which works on the original training set without extra data collection process. We first expand the training set with unlabeled data using GAN. Then our model minimizes the sum of the supervised and the unsupervised losses through a new regularization scheme. This method is evaluated in person re-identification [46] which aims at spotting the target person in different cameras and is recently viewed as an image retrieval problem [47].

This work addresses three challenges. First, current re-

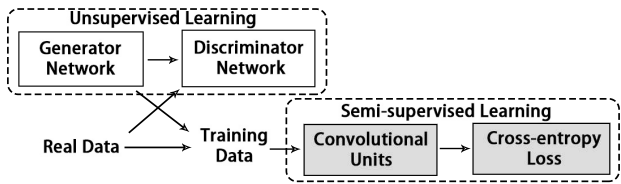


Figure 1. The pipeline of the proposed method. There are two components: a generative adversarial model [23] for unsupervised learning and a convolutional neural network for semi-supervised learning. “Real Data” represents the labeled data in the given training set; “Training data” includes both the “Real Data” and the generated unlabeled data. We aim to learn more discriminative embeddings with the “Training data”.

search in GAN typically considers the quality of sample generation w/wo semi-supervised learning *in vivo* [27, 23, 5, 22, 16, 36]. Yet a scientific problem remains mostly unknown how to move the generated samples out of box and use them in currently available learning frameworks. To this end, this work uses unlabeled data produced by the DCGAN model [23], in together with the labeled training data. As shown in Fig. 1, our pipeline feeds the newly generated samples into another learning machine (CNN). We therefore use the term “*in vitro*” to differentiate our method from [27, 23, 5] which perform semi-supervised learning in the Discriminator of GAN (*in vivo*).

Second, it remains challenging how to perform semi-supervised learning using labeled and unlabeled data in CNN-based methods. Usually the unsupervised data is used as a pre-training step before supervised learning [24, 9, 12], while our method uses all the data simultaneously. In [21, 17, 27], the unlabeled/weakly labeled data are assigned some labels according to the pre-defined training classes. These methods are different from our task in that technically the GAN generated data does not belong to any of the existing classes (especially in person re-ID, see Fig. 2). The proposed LSRO does not include unsupervised pre-training nor label assignment to the known classes. We address semi-

supervised learning in a new perspective: since the unlabeled samples do not belong to any of the existing labeled classes, they are assigned a uniform label distribution over the training classes.

Third, in person re-ID, data annotation is expensive, because one has to draw a pedestrian bounding box and assign an ID label to it. Recent progress in this field can be attributed due to two factors: 1) the availability of large-scale re-ID datasets [45, 48, 40, 18] and 2) the learned embedding of pedestrian using a convolutional neural network (CNN) [6, 8]. That being said, the number of images of each identity is still limited. There are 17.2 images per identities in Market1501 [45] and 9.6 images in CUHK03 [18] on average. So using additional data is non-trivial to avoid model over-fitting. In literature, usually pedestrian images used in training are provided by the training sets, without being expanded. So it is mostly unknown if a larger training set with unlabeled images brings extra benefit. This inspired us to resort to the GAN samples to enlarge and enrich the training set and employs the proposed regularization to implement a semi-supervised system.

In the attempt on the above-mentioned challenges, this paper 1) adopts GAN in unlabeled data generation, 2) proposes the label smoothing regularization for outliers (LSRO) for unlabeled data integration, and 3) reports improvement over a CNN baseline on two person re-ID datasets. In more details, in the first step, we train DCGAN [23] on the original re-ID training set. We generate new pedestrian images by inputting random 100-dim vectors in which each entry falls within $[-1, 1]$. Some generated samples are shown in Fig. 2 and Fig. 4. In the second step, these unlabeled GAN-generated data are fed into the ResNet model. LSRO regularizes the learning process by integrating the unlabeled data and thus reduces the risk of over-fitting. Finally, we evaluate the proposed method on person re-identification and show that the learned embeddings demonstrate consistent improvement over the ResNet baseline.

To summarize, our contributions are:

- We introduce a semi-supervised pipeline which integrates GAN-generated images into the CNN learning machine *in vitro*.
- We propose the label smoothing regularization for outliers (LSRO) for semi-supervised learning. The integration of unlabeled data regularizes the CNN learning process. We show that LSRO is superior to two available strategies for dealing with unlabeled data.
- We show that the proposed semi-supervised pipeline demonstrates consistent improvement over the ResNet baseline on two person re-ID datasets.



Figure 2. Examples of GAN images and real images. (a) The top two rows show the pedestrian samples generated by DCGAN [23] trained on the Market1501 training set [45]. (b) The bottom row shows the real samples in training set. Although the generated images in (a) can be easily recognized as fake images by human, they still serve as an effective regularizer in our experiment.

2. Related work

In this section we will discuss the related works in the generative adversarial networks (GANs), semi-supervised learning and person re-ID.

2.1. Generative Adversarial Networks

The generative adversarial networks (GANs) learn two sub-networks: the Generator and the Discriminator. The Discriminator is to tell whether a sample is generated or real. The Generator is to generate visually real samples to cheat the discriminator. The GANs are first proposed by Goodfellow *et al.* [10] to generate images and gain insights into the neural network. Then, DCGAN [23] provides some techniques to improve the stability of training. The discriminator of DCGAN can serve as a robust feature extractor. Salimans *et al.* [27] achieve the state-of-art result in semi-supervised classification and meanwhile improve the visual quality of GANs. InfoGAN [5] learns interpretable representations by introducing latent codes. On the other hand, GANs also demonstrate potential in generating images for specific fields. Pathak *et al.* [22] propose an encoder-decoder method to image inpainting. GANs are used as the image generative model. Similarly, Yeh *et al.* [41] improve the inpainting performance by introducing two loss types. Ledig *et al.* [16] use GANs to tackle the super-resolution problem. In [36], 3D object images are generated by a 3D-GAN. In this work, we do not focus on investigating more sophisticated sample generation methods. Instead, we use a basic GAN model [23] to generate unlabeled samples from the training data and show that these samples help improve the discriminative learning.

2.2. Semi-supervised learning

Semi-supervised learning is a sub-class of supervised learning taking unlabeled data into consideration, especially when the volume of annotated data is small. On the one hand, some research treats unsupervised learning as an auxiliary task to the supervised learning. For example, in [12], Hinton *et al.* learn a stack of unsupervised restricted Boltzmann machines to pre-train the model. Ranzato *et al.* propose to reconstruct the input at every level of network to get compact representative [24]. In [25] the auxiliary task of Ladder network is to denoise representations at every level of the model. On the other hand, several works assign some labels to the unlabeled data. Papandreou *et al.* [21] combine strong and weak labels in CNN using an expectation-maximization (EM) process for image segmentation. In [17], Lee assigns a “pseudo label” to the unlabeled data with the class which has the maximum predicted probability. In [27], the samples produced by the Generator of GAN are all taken as one class in the Discriminator. Departing from previous semi-supervised works, we adopt a different regularization approach by assigning a uniform label distribution to the generated samples.

2.3. Person Re-identification

Recent progress in person re-ID mainly consists in the advance of the convolutional neural network (CNN). Yi *et al.* [42] split a pedestrian image into three horizontal parts and respectively train three part-CNNs to extract features. Similarly, Cheng *et al.* [6] split the convolutional map into four parts and fuse the part features with the global feature. In [18], Li *et al.* add a new layer that multiplies the activation of two images in different horizontal stripes. They use this layer to explicitly allow patch matching in CNN. Later, Ahmed *et al.* [2] improve the performance by proposing a new patch matching layer that compares the activation of two images in neighboring pixels. Besides, Varior *et al.* [31] combine CNN with some gate functions, aiming to adaptively focus on the salient parts of input image pairs, but this method is limited by the computational inefficiency because the input should be image pairs.

CNN can be very discriminative by itself without explicit part-matching. Zheng *et al.* [46, 48, 44] directly use a conventional fine-tuning approach (called the ID-discriminative Embedding, or IDE) on Market1501 [45] and MARS [44] and the performance outperforms many other recent results. Wu *et al.* [39] combine the CNN embedding with hand-crafted features. In [49], Zheng *et al.* combine the identification model with the verification model and improve the fine-tuned CNN performance. In this paper, we adopt the IDE model [46, 48] as baseline, and show that the GAN samples and LSRO effectively improves its performance. Recently, Barbosa *et al.* [3] propose to synthesize human images through a photorealistic body generation

software. These images are used to pre-train an IDE model before dataset-specific fine-tuning. Our method is different from [3] in both data generation and the training strategy.

3. Network Overview

In this section, we describe the pipeline of the proposed method. As shown in Fig. 1, we first use the real data in the training set to train the generative adversarial network (GAN) model. We then combine the real training data and the newly generated samples as the training input of the convolutional neural network (CNN). In the following section, we will illustrate the structure of the two components, *i.e.*, GAN and CNN, in details. Note that, **except that the number of neurons of the last FC layer in CNN is modified according to the number of training classes, our system does not make major changes to the network structures of GAN and CNN.**

3.1. Generative Adversarial Network

The generative adversarial network has two components: the Generator and Discriminator. For the Generator, we follow the settings in [23]. We start with a 100-dim random vector and enlarge it to $4 \times 4 \times 16$ by a linear function. To enlarge the tensor, we then use five deconvolution functions whose kernel size is 5×5 and stride is 2. Every deconvolution is followed by ReLU and Batch Normalization. Additionally, we add one optional deconvolutional layer whose kernel size is 5×5 and stride is 1, and one *tanh* function to fine-tune the result. Finally, we can obtain a generated sample of size $128 \times 128 \times 3$.

For the Discriminator network, the input includes the generated images and the real images in training set. We use five convolutional layer to classify whether the generated image is fake. Similarly, the size of the convolutional filters is 5×5 and stride is 2. We add a fully connected layer to do binary classification.

3.2. Convolutional Neural Network

The ResNet-50 [11] model is used in our experiment. We resize the generated images to $256 \times 256 \times 3$ by bilinear sampling. The generated images are mixed with the original training set as the input of CNN. That is, the labeled and unlabeled data are simultaneously trained. These training images are shuffled. Following the conventional fine-tuning strategy [44, 46], we use the model pretrained on ImageNet [26]. We modify the last fully connected (FC) layer to have K neurons to predict the K -classes, where K is the number of the classes in the original training set (also the merged new training set). Different from [27], we do not view the new samples as an extra class, but assign a uniform label distribution over the existing classes. So the last FC layer remains K -dimensional. The assigned label distribution of the generated images will be discussed in the next section.

4. The Proposed Regularization Scheme

In this section, we will first revisit the label smoothing regularization (LSR), which is used for fully supervised learning. We then extend LSR to the scenario of unlabeled learning, yielding the so-called label smoothing regularization for outliers (LSRO) scheme.

4.1. Label Smoothing Regularization Revisit

LSR was proposed in 1980s and recently re-discovered by Szegedy *et al.* [29]. In a nutshell, LSR assigns small values to the non-groundtruth classes instead of 0. This discourages the network to be tuned towards the groundtruth class and thus reduces the chances of over-fitting. LSR is proposed to be used with the cross-entropy loss [29].

Formally, let $k \in \{1, 2, \dots, K\}$ be the pre-defined classes of the training data, where K is the number of classes. The cross-entropy loss can be formulated as:

$$l = - \sum_{k=1}^K \log(p(k))q(k), \quad (1)$$

where $p(k) \in [0, 1]$ is the predicted probability of the input belonging to class k , and can be outputted by CNN. It is obtained by the softmax function which normalizes the output of the previous FC layer. $q(k)$ is the groundtruth distribution. Let y be the groundtruth class label, $q(k)$ can be defined as:

$$q(k) = \begin{cases} 0 & k \neq y \\ 1 & k = y \end{cases}. \quad (2)$$

If we discard the zero terms in Eq. 1, the cross-entropy loss is equivalent to that only considering the groundtruth term as Eq. 3.

$$l = -\log(p(y)). \quad (3)$$

So minimizing the cross-entropy loss is equivalent to maximizing the predicted probability of the ground-truth class. In [29], the label smoothing regularization (LSR) is introduced to take into account the distribution of the non-groundtruth classes. The network is thus encouraged not to be too confident towards the groundtruth. In [29], the label distribution $q_{LSR}(k)$ is written as:

$$q_{LSR}(k) = \begin{cases} \frac{\varepsilon}{K} & k \neq y \\ 1 - \varepsilon + \frac{\varepsilon}{K} & k = y \end{cases}, \quad (4)$$

where $\varepsilon \in [0, 1]$ is a hyper parameter. If ε is zero, Eq. 4 reduces to Eq. 2. If ε is too large, the model may fail to predict the groundtruth label. So in usual cases, ε is set to 0.1. Szegedy *et al.* assume that the non-groundtruth classes take on a uniform label distribution. Considering Eq. 1 and Eq. 4, the cross-entropy loss evolves to:

$$l_{LSR} = -(1 - \varepsilon) \log(p(y)) - \frac{\varepsilon}{K} \sum_{k=1}^K \log(p(k)). \quad (5)$$

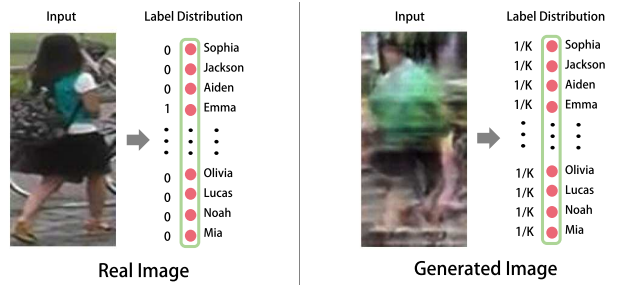


Figure 3. The label distributions of a real image and a GAN-generated image in our system. For the real image (left), we use a classical label distribution (Eq. 2). For the generated image (right), we employ the proposed LSRO label distribution (Eq. 6), *e.g.* a uniform distribution on every training class because the generated image is assumed to belong to none of the training classes. We employ a cross-entropy loss that combines the two types of label distributions as the optimization objective (Eq. 7).

Comparing with Eq. 3, Eq. 5 pays additional attention to the other classes rather than only the groundtruth class. In this paper, we do not employ LSR on the IDE baseline, because it yields slightly lower performance than using Eq. 2 (see Section 5.3). We re-introduce LSR because it inspires us in designing the LSRO method.

4.2. Label Smoothing Regularization for Outliers

In this paper, we propose the label smoothing regularization for outliers (LSRO) to incorporate the unlabeled images in the network. It extends LSR from the supervised domain to leveraging the unsupervised data generated by GAN.

In LSRO, we propose a virtual label distribution for the unlabeled images. We set the virtual label distribution to be uniform over the K classes, due to two inspirations. 1) We assume that the generated samples do not belong to any pre-defined classes. 2) LSR assumes a uniform distribution over the non-groundtruth classes to address over-fitting. During testing, we expect that the maximum class probability of a generated image is low, *i.e.*, the network fails to predict a class with high confidence. Formally, for a generated image, its class label distribution, $q_{LSRO}(k)$, is defined as:

$$q_{LSRO}(k) = \frac{1}{K}. \quad (6)$$

We name Eq. 6 the label smoothing regularization for outliers (LSRO).

For the real images in the training set, we still use the one-hot distribution defined in Eq. 2 for the loss computation. Combining Eq. 2, Eq. 6 and Eq. 1, we can re-write the cross-entropy loss as:

$$l_{LSRO} = -(1 - Z) \log(p(y)) - \frac{Z}{K} \sum_{k=1}^K \log(p(k)). \quad (7)$$

For a real training image, $Z = 0$. For a generated training image, $Z = 1$. So our system actually has two types of losses for the real images and generated images, respectively.

Advantage of LSRO. With LSRO, we have more training images (outliers) that locate near the real training images in the sample space, and introduce more color, lighting and pose variances to regularize model training. For instance, if we only have one green-clothed identity in the training set, the network may be confused into considering that green color is a discriminative feature. So it limits the discriminative ability of the model. By adding generated training samples such as an unlabeled green-clothed person, we will penalize the classifier if it makes the wrong prediction towards the labeled green-clothed person. By this manner, we encourage the network to find more robust features and to be less prone to over-fitting. In this work, we only use GAN trained on the original training set to produce outlier images; it is an interesting idea to further evaluate if real-world unlabeled images can achieve similar effects (see Table 3).

Competing methods. We compare LSRO with two alternative methods in this paper. Both methods can be accessed from existing literature [27, 17].

- **All in one.** Following [27], we create a new class label, *i.e.*, $K + 1$, and every generated sample is assigned to this class. CNN training follows Section 5.2.
- **Pseudo label.** Following [17], during network training, each incoming GAN-image is passed forward through the current network and is assigned a pseudo label by taking the maximum value of the probability prediction vector ($p(k)$ in Eq. 1). This GAN-image can be thus trained in the network with this pseudo label. During training, the pseudo label is assigned *dynamically*, so that the same GAN-image may receive different pseudo labels each time it is fed into the network. In experiment, we start feeding GAN images and assigning them pseudo labels after 20 epochs. We set a global weight to the softmax loss of the GAN and real images, *i.e.*, 0.1 and 1.

Our experimental results show that the two methods also work on the GAN images, and that LSRO is superior to “All in one” and “Pseudo label”. We will provide explanations in the Section 5.3.

5. Experiment

We mainly evaluate the proposed method on the Market1501 [45] dataset, because it has a large scale and a fixed train/test split. We also report results on the CUHK03 dataset [18], **but due to the computational cost of 20 train/test splits, we only use the GAN model trained on Market1501.**

5.1. Dataset

Market1501 is a large-scale person re-ID dataset collected from six cameras, which contains 19,732 images for testing and 12,936 images for training. The images are automatically detected by the deformable part model (DPM) [7], so the mis-alignment is common and the dataset is close to realistic settings. There are 751 identities in the training set and 750 identities in the testing set. The number of the images of the training identities is 17.2 on average. We use all the 12,936 detected images from the training set to train the GAN model. We use 90% of the training data to for training and 10% for validation.

CUHK03 contains 14,097 images of 1,467 identities. Each identity is captured by two cameras in the CUHK campus. It provides two image sets. One is annotated by hand-drawn bounding boxes and the other is produced by the DPM detector [7]. We use the detected set in this paper. The number of images of the training identities is 9.6 on average. We report the averaged result after training/testing 20 times. We use the **single shot** setting.

5.2. Implementation details

CNN Re-ID baseline. We adopt the CNN re-ID baseline used in [46, 44, 48]. Specifically, the Matconvnet [33] package is used. During training, We use the ResNet-50 model [11] and modify the FC layer to have 751 and 1,367 neurons for Market1501 and CUHK03, respectively. All the images are resized to 256×256 before being randomly cropped into 224×224 with random horizontal flipping. We insert a dropout layer [13] before the final convolutional layer and set the dropout rate to 0.5 for CUHK03 and 0.75 for Market1501, respectively. The ImageNet pre-trained ResNet model is used for fine-tuning. We use stochastic gradient descent with momentum 0.9. The learning rate of the convolution layers is set to 0.002 and decay to 0.0002 after 40 epochs and we stop training after the 50 epochs. During testing, we extract the 2,048-dim CNN embedding in the last convolutional layer for an input image of size 224×224 . The similarity between two images is calculated by cosine distance before ranking.

GAN training and testing. We use Tensorflow [1] and the DCGAN package¹ to train the GAN model. For training GAN, we use the provided data in the Market1501 training set without preprocessing (*e.g.* foreground detection). All the images are resized to 128×128 and randomly flipped before training. We use Adam [14] with parameters $\beta_1 = 0.5$, $\beta_2 = 0.99$. We stop training after 30 epochs. During GAN testing, we randomly input a 100-dim vector in GAN, and the value of each entry ranges in $[-1, 1]$. The outputted image is used in CNN training (with LSRO). More GAN images are shown in Fig. 4.

¹<https://github.com/carpedm20/DCGAN-tensorflow>

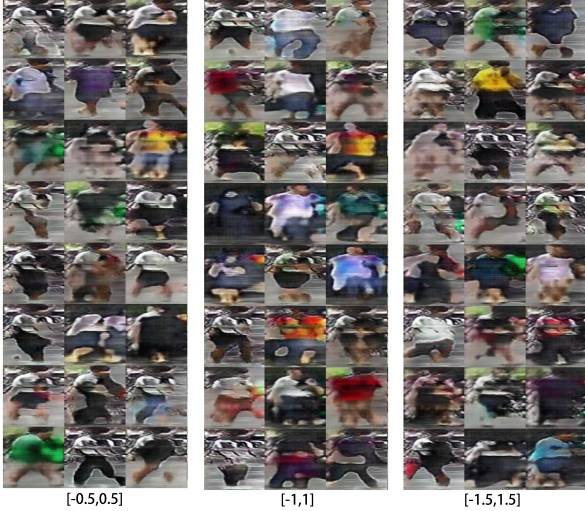


Figure 4. The newly generated images from a DCGAN model trained on Market1501. Through LSRO, they are added to the training sets of Market1501 and CUHK03 to regularize the CNN model. Here, we show GAN images that are generated by different scales of the random vector, *i.e.* $[-0.5, 0.5]$, $[-1, 1]$, $[-1.5, 1.5]$. We hardly find any significant visual differences among them.

5.3. Evaluation

The ResNet baseline. Using the training/testing procedure described in Section 5.2, we report the baseline performance of ResNet in Table 4 and Table 5. The rank-1 accuracy is 73.69% and 71.5% on Market-1501 and CUHK03 respectively. Our baseline results are on par with the those reported in [46, 49]. Note that the baseline alone exceeds many previous works [32, 37, 43].

We have also trained a baseline ResNet model using the label smoothing regularizaton (LSR) with $\varepsilon = 0.1$ (see Eq. 4 in Section 4.1). We obtain a 72.90% rank-1 precision and 50.57% mAP, which is slightly lower than using the standard one-hot cross-entropy loss. Therefore LSR has limited positive effect on Market1501 [45]. Considering this, and the fact that LSRO works on Market1501 (to be illustrated later) suggest that LSRO has a distinct working mechanism with LSR, and that the design of LSRO is not trivial. In the following experiment, we do not apply LSR.

The GAN images improve the baseline. As shown in Table 1, when we add 24,000 GAN images to CNN training, our method significantly improves the re-ID performance on Market1501. We observe improvement of +4.37% (from 73.69% to 78.06%) and +4.75% (from 51.48% to 56.23%) in rank-1 accuracy and mAP, respectively. On CUHK03, we observe improvement of +1.6%, +1.2%, +0.8%, and +1.6% in rank-1, 5, 10 accuracy and mAP, respectively. The improvement on CUHK03 is relatively small compared to that of CUHK03, because the DC-

# GAN Img.	LSRO		All in one		Pseudo label	
	rank-1	mAP	rank-1	mAP	rank-1	mAP
0 (basel.)	73.69	51.48	73.69	51.48	73.69	51.48
12,000	76.81	55.32	75.33	52.82	76.07	53.56
18,000	77.26	55.55	77.20	55.04	76.34	53.45
24,000	78.06	56.23	76.63	55.12	75.80	53.03
30,000	77.38	55.48	75.95	55.18	75.21	52.65
36,000	76.07	54.59	76.87	55.47	74.67	52.38

Table 1. Comparison of LSRO, “All in one”, and “Pseudo label” under different numbers of GAN-generated images on Market1501. We show that LSRO is superior to the other two methods whose best performance is highlighted in blue and red, resp. Rank-1 accuracy (%) and mAP (%) are shown.

Random Range	rank-1	mAP
$[-0.5, 0.5]$	0.7705	0.5556
$[-1, 1]$	0.7806	0.5623
$[-1.5, 1.5]$	0.7785	0.5573

Table 2. We use different ranges to produce the random vectors as input to GAN. The resulting GAN images are tested in our system. We show the rank-1 accuracy (%) and mAP (%) on Market1501.

GAN model is trained on Market-1501 and the generated images share more similar distribution with Market-1501 than CUHK03. These results indicate that the unlabeled images generated by GAN effectively yield improvement over the baseline under LSRO.

The impact of using different numbers of GAN images during training. We then evaluate how the number of GAN images affects the final re-ID performance. Experimental results on Market1501 are shown in Table 1. We note that the number of real training images in Market1501 is 12,936. Two observations are made.

First, the addition of different numbers of GAN images consistently improves the baseline. Adding approximately 3x GAN images compared to the real training set still has a +2.38% improvement in rank-1 accuracy.

Second, we observe the peak performance is achieved when 2x GAN images are added. On the one hand, when too few GAN sample are incorporated in the system, the regularization ability of LSRO is inadequate. On the other hand, when too many GAN samples are present, the learning machine tends to converge towards assigning uniform prediction probabilities to all the training samples, which is not desirable either. Therefore, a trade-off is recommended to avoid poor regularization and over-fitting to uniform label distributions.

Impact of the scale of the random vectors inputted in GAN. We evaluate whether the scale of the random vector – the input of GAN – impacts the classification result. In the generator of the GAN model, we use the 100-dim random codes to generate the samples. To verify the impact, we try

Unsup. Data	rank-1	mAP
0 (basel.)	0.7369	0.5148
CUHK03-Real-12000	0.7565	0.5325
Market1501-GAN-12000	0.7681	0.5532

Table 3. We add the 12000 real pedestrian images in CUHK03 as the outlier to Market1501 dataset. We find the model trained on the generated samples out-performs the model trained on CUHK03 real data. Rank-1 accuracy (%) and mAP (%) are shown.

Method	Single Query		Multi. Query	
	rank-1	mAP	rank-1	mAP
BoW+kissme [45]	44.42	20.76	-	-
SL [4]	51.90	26.35	-	-
MR CNN [30]	45.58	26.11	56.59	32.26
DADM [28]	39.4	19.6	49.0	25.8
CAN [20]	48.24	24.43	-	-
DNS [43]	55.43	29.87	71.56	46.03
FisherNet [38]	48.15	29.94	-	-
S-LSTM [32]	-	-	61.6	35.3
Gate Reid [31]	65.88	39.55	76.04	48.45
Verif.-Classif. [49]*	79.51	59.87	85.84	70.33
DeepTransfer [8]*	83.7	65.5	89.6	73.8
SOMAnet [3]*	73.87	47.89	81.29	56.98
ResNet Basel. [46]*	73.69	51.48	81.47	63.95
Ours	78.06	56.23	85.12	68.52

Table 4. Comparison with the state-of-the-art methods reported on the Market1501 dataset. We also provide results of the fine-tuned ResNet baseline. Rank-1 precision (%) and mAP (%) are listed. * the respective paper is on ArXiv but not published.

different ranges of the random code, *i.e.*, $[-0.5, 0.5]$, $[-1, 1]$, and $[-1.5, 1.5]$, with a zero-mean distribution. Typically, a larger range may contain some rare and strange patterns and a smaller range may limit the variations in the generated images. The experimental results on Market1501 are shown in Table 2. and the visual examples are shown in Fig. 4. We find that the visual examples do not show obvious differences between three ranges, and that $[-1, 1]$ yields slightly higher re-ID performance than the other two.

GAN images vs. real images in training. To further evaluate the proposed method, we replace the GAN images with the real images from the CUHK03 dataset which are viewed as unlabeled in the experiment. Since CUHK03 only 14,097 images, we randomly select 12,000 for fair comparison.

Experimental results are shown in Table 3. We compare the results obtained using the 12,000 CUHK03 images and the 12,000 GAN images. We find the real data from CUHK03 also assists in the regularization and improves the performance. But the model trained with GAN-generated data is slightly better. In fact, although the images generated from DCGAN are visually imperfect (see Fig. 2), they still

Methods	rank-1	rank-5	rank-10	mAP
KISSME [15]	11.7	33.3	48.0	-
DeepReID [18]	19.9	49.3	64.7	-
BoW+HS [45]	24.3	-	-	-
LOMO+XQDA [19]	46.3	78.9	88.6	-
SI-CI [34]	52.2	84.3	94.8	-
DNS [43]	54.7	80.1	883.	-
Verif.-Classif [49]*	66.1	90.1	95.5	71.2
DeepTransfer [8]*	84.1	-	-	-
SOMAnet [3]*	72.4	92.1	95.8	-
ResNet Basel. [46]*	71.5	91.5	95.9	75.8
Ours	73.1	92.7	96.7	77.4

Table 5. Comparison with the state-of-the-art reports on the CUHK03 dataset. We list the fine-tuned ResNet baseline as well. The mAP (%) and rank1 (%) precision are presented. * the respective paper is on ArXiv but not published.

possess similar regularization ability as the real images. We will present more experiment *w.r.t* this problem.

Comparison with two competing methods. We compare LSRO with the “All in one” and “Pseudo label” methods implied in [27] and [17], respectively. The experimental results on Market1501 are summarized in Table 1.

We first observe that both strategies yield improvement over the baseline. For the “All in one” method, it treats all the unlabeled samples as a new class, so it forces the network to make “careful” predictions for the existing K classes. The “Pseudo label” method gradually labels the new data, and thus introduces more variance to the network.

Nevertheless, we find that LSRO exceeds both strategies by $+1\% \sim +2\%$. We speculate the reason is that the “All in one” method makes a coarse label estimation, while “Pseudo label” originally assumes that all the unlabeled data belongs to the existing classes [17] which is not true in person re-ID. While these two methods still use the one hot label distribution, the LSRO method makes less stronger assumption (label smoothing) towards the labels of the GAN images. These reasons may explain why LSRO has a superior performance.

Comparison with the state of the art. We compare our result with the state of the art in Table 4 and Table 5, respectively. On the Market-1501 dataset, we achieve **rank-1 accuracy = 78.06%, mAP = 56.23%** when using the single query mode, which is the best result compared with published papers, and the second best among all the available results including ArXiv papers. On the CUHK03 dataset, we arrive at **rank-1 accuracy = 73.1%, mAP = 77.4%** which is also very competitive. We envision that the techniques used in [8, 49] may be complementary to our system.

6. Conclusion

In this paper, we propose an “in vitro” usage of the generative adversarial networks (GANs) in discriminative learning, *i.e.*, person re-identification. Using a baseline DCGAN model [23], we show that the imperfect GAN images effectively demonstrate their regularization ability when trained in the ResNet baseline network. Through the proposed label smoothing regularization for outliers (LSRO) scheme, the unlabeled GAN images are mixed with the labeled real training images for simultaneous semi-supervised learning. Albeit simple, we demonstrate consistent performance improvement over the re-ID baseline system, which sheds light on the effective usage of the GAN generated data.

Two important issues remains to be addressed. First, do GAN images of better visual quality yield superior results when integrated in supervise learning? This paper provides some baseline evaluations using the imperfect GAN images, and future investigations would be intriguing. Second, will the GAN images work in other fields such as fine-grained classification or instance retrieval? According to our preliminary results, our method is challenging to work on the CUB-200-2011 dataset [35]. But we believe more effective training strategies will do.

References

[1] M. Abadi, P. Barham, J. Chen, Z. Chen, A. Davis, J. Dean, M. Devin, S. Ghemawat, G. Irving, M. Isard, et al. Tensorflow: A system for large-scale machine learning. In *Proceedings of the 12th USENIX Symposium on Operating Systems Design and Implementation (OSDI)*, 2016. 5

[2] E. Ahmed, M. Jones, and T. K. Marks. An improved deep learning architecture for person re-identification. In *Proceedings of the IEEE Conference on Computer Vision and Pattern Recognition*, pages 3908–3916, 2015. 3

[3] I. B. Barbosa, M. Cristani, B. Caputo, A. Rognhaugen, and T. Theoharis. Looking beyond appearances: Synthetic training data for deep cnns in re-identification. *arXiv preprint arXiv:1701.03153*, 2017. 3, 7

[4] D. Chen, Z. Yuan, B. Chen, and N. Zheng. Similarity learning with spatial constraints for person re-identification. In *Proceedings of the IEEE Conference on Computer Vision and Pattern Recognition*, pages 1268–1277, 2016. 7

[5] X. Chen, Y. Duan, R. Houthooft, J. Schulman, I. Sutskever, and P. Abbeel. Infogan: Interpretable representation learning by information maximizing generative adversarial nets. In *Advances in Neural Information Processing Systems*, pages 2172–2180, 2016. 1, 2

[6] D. Cheng, Y. Gong, S. Zhou, J. Wang, and N. Zheng. Person re-identification by multi-channel parts-based cnn with improved triplet loss function. In *Proceedings of the IEEE Conference on Computer Vision and Pattern Recognition*, pages 1335–1344, 2016. 2, 3

[7] P. F. Felzenszwalb, R. B. Girshick, D. McAllester, and D. Ramanan. Object detection with discriminatively trained part-based models. *IEEE transactions on pattern analysis and machine intelligence*, 32(9):1627–1645, 2010. 5

[8] M. Geng, Y. Wang, T. Xiang, and Y. Tian. Deep transfer learning for person re-identification. *arXiv preprint arXiv:1611.05244*, 2016. 2, 7

[9] I. Goodfellow, M. Mirza, A. Courville, and Y. Bengio. Multi-prediction deep boltzmann machines. In *Advances in Neural Information Processing Systems*, pages 548–556, 2013. 1

[10] I. Goodfellow, J. Pouget-Abadie, M. Mirza, B. Xu, D. Warde-Farley, S. Ozair, A. Courville, and Y. Bengio. Generative adversarial nets. In *Advances in Neural Information Processing Systems*, pages 2672–2680, 2014. 2

[11] K. He, X. Zhang, S. Ren, and J. Sun. Deep residual learning for image recognition. In *Proceedings of the IEEE Conference on Computer Vision and Pattern Recognition*, pages 770–778, 2016. 3, 5

[12] G. E. Hinton and R. R. Salakhutdinov. Reducing the dimensionality of data with neural networks. *science*, 313(5786):504–507, 2006. 1, 3

[13] G. E. Hinton, N. Srivastava, A. Krizhevsky, I. Sutskever, and R. R. Salakhutdinov. Improving neural networks by preventing co-adaptation of feature detectors. *arXiv preprint arXiv:1207.0580*, 2012. 5

[14] D. Kingma and J. Ba. Adam: A method for stochastic optimization. *arXiv preprint arXiv:1412.6980*, 2014. 5

[15] M. Köstinger, M. Hirzer, P. Wohlhart, P. M. Roth, and H. Bischof. Large scale metric learning from equivalence constraints. In *Computer Vision and Pattern Recognition (CVPR), 2012 IEEE Conference on*, pages 2288–2295. IEEE, 2012. 7

[16] C. Ledig, L. Theis, F. Huszár, J. Caballero, A. Cunningham, A. Acosta, A. Aitken, A. Tejani, J. Totz, Z. Wang, et al. Photo-realistic single image super-resolution using a generative adversarial network. *arXiv preprint arXiv:1609.04802*, 2016. 1, 2

[17] D.-H. Lee. Pseudo-label: The simple and efficient semi-supervised learning method for deep neural networks. In *Workshop on Challenges in Representation Learning, ICML*, volume 3, page 2, 2013. 1, 3, 5, 7

[18] W. Li, R. Zhao, T. Xiao, and X. Wang. Deepreid: Deep filter pairing neural network for person re-identification. In *Proceedings of the IEEE Conference on Computer Vision and Pattern Recognition*, pages 152–159, 2014. 1, 2, 3, 5, 7

[19] S. Liao, Y. Hu, X. Zhu, and S. Z. Li. Person re-identification by local maximal occurrence representation and metric learning. In *Proceedings of the IEEE Conference on Computer Vision and Pattern Recognition*, pages 2197–2206, 2015. 7

[20] H. Liu, J. Feng, M. Qi, J. Jiang, and S. Yan. End-to-end comparative attention networks for person re-identification. *arXiv preprint arXiv:1606.04404*, 2016. 7

[21] G. Papandreou, L.-C. Chen, K. P. Murphy, and A. L. Yuille. Weakly-and semi-supervised learning of a deep convolutional network for semantic image segmentation. In *Proceedings of the IEEE International Conference on Computer Vision*, pages 1742–1750, 2015. 1, 3

[22] D. Pathak, P. Krahenbuhl, J. Donahue, T. Darrell, and A. A. Efros. Context encoders: Feature learning by inpainting. In *Proceedings of the IEEE Conference on Computer Vision and Pattern Recognition*, pages 2536–2544, 2016. [1](#), [2](#)

[23] A. Radford, L. Metz, and S. Chintala. Unsupervised representation learning with deep convolutional generative adversarial networks. *arXiv preprint arXiv:1511.06434*, 2015. [1](#), [2](#), [3](#), [8](#)

[24] M. Ranzato and M. Szummer. Semi-supervised learning of compact document representations with deep networks. In *Proceedings of the 25th international conference on Machine learning*, pages 792–799. ACM, 2008. [1](#), [3](#)

[25] A. Rasmus, M. Berglund, M. Honkala, H. Valpola, and T. Raiko. Semi-supervised learning with ladder networks. In *Advances in Neural Information Processing Systems*, pages 3546–3554, 2015. [1](#), [3](#)

[26] O. Russakovsky, J. Deng, H. Su, J. Krause, S. Satheesh, S. Ma, Z. Huang, A. Karpathy, A. Khosla, M. Bernstein, et al. Imagenet large scale visual recognition challenge. *International Journal of Computer Vision*, 115(3):211–252, 2015. [3](#)

[27] T. Salimans, I. Goodfellow, W. Zaremba, V. Cheung, A. Radford, and X. Chen. Improved techniques for training gans. In *Advances in Neural Information Processing Systems*, pages 2226–2234, 2016. [1](#), [2](#), [3](#), [5](#), [7](#)

[28] C. Su, S. Zhang, J. Xing, W. Gao, and Q. Tian. Deep attributes driven multi-camera person re-identification. In *European Conference on Computer Vision*, pages 475–491. Springer, 2016. [7](#)

[29] C. Szegedy, V. Vanhoucke, S. Ioffe, J. Shlens, and Z. Wojna. Rethinking the inception architecture for computer vision. In *Proceedings of the IEEE Conference on Computer Vision and Pattern Recognition*, pages 2818–2826, 2016. [4](#)

[30] E. Ustinova, Y. Ganin, and V. Lempitsky. Multiregion bilinear convolutional neural networks for person re-identification. *arXiv preprint arXiv:1512.05300*, 2015. [7](#)

[31] R. R. Varior, M. Haloi, and G. Wang. Gated siamese convolutional neural network architecture for human re-identification. In *European Conference on Computer Vision*, pages 791–808. Springer, 2016. [3](#), [7](#)

[32] R. R. Varior, B. Shuai, J. Lu, D. Xu, and G. Wang. A siamese long short-term memory architecture for human re-identification. In *European Conference on Computer Vision*, pages 135–153. Springer, 2016. [6](#), [7](#)

[33] A. Vedaldi and K. Lenc. Matconvnet – convolutional neural networks for matlab. In *Proceeding of the ACM Int. Conf. on Multimedia*, 2015. [5](#)

[34] F. Wang, W. Zuo, L. Lin, D. Zhang, and L. Zhang. Joint learning of single-image and cross-image representations for person re-identification. [7](#)

[35] P. Welinder, S. Branson, T. Mita, C. Wah, F. Schroff, S. Belongie, and P. Perona. Caltech-UCSD Birds 200. Technical Report CNS-TR-2010-001, California Institute of Technology, 2010. [8](#)

[36] J. Wu, C. Zhang, T. Xue, B. Freeman, and J. Tenenbaum. Learning a probabilistic latent space of object shapes via 3d generative-adversarial modeling. In *Advances in Neural Information Processing Systems*, pages 82–90, 2016. [1](#), [2](#)

[37] L. Wu, C. Shen, and A. v. d. Hengel. Personnet: Person re-identification with deep convolutional neural networks. *arXiv preprint arXiv:1601.07255*, 2016. [6](#)

[38] L. Wu, C. Shen, and A. van den Hengel. Deep linear discriminant analysis on fisher networks: A hybrid architecture for person re-identification. *Pattern Recognition*, 2016. [7](#)

[39] S. Wu, Y.-C. Chen, X. Li, A.-C. Wu, J.-J. You, and W.-S. Zheng. An enhanced deep feature representation for person re-identification. In *2016 IEEE Winter Conference on Applications of Computer Vision (WACV)*, pages 1–8. IEEE, 2016. [3](#)

[40] T. Xiao, S. Li, B. Wang, L. Lin, and X. Wang. End-to-end deep learning for person search. *arXiv preprint arXiv:1604.01850*, 2016. [2](#)

[41] R. Yeh, C. Chen, T. Y. Lim, M. Hasegawa-Johnson, and M. N. Do. Semantic image inpainting with perceptual and contextual losses. *arXiv preprint arXiv:1607.07539*, 2016. [2](#)

[42] D. Yi, Z. Lei, and S. Z. Li. Deep metric learning for practical person re-identification. *arXiv preprint arXiv:1407.4979*, 2014. [3](#)

[43] L. Zhang, T. Xiang, and S. Gong. Learning a discriminative null space for person re-identification. *arXiv preprint arXiv:1603.02139*, 2016. [6](#), [7](#)

[44] L. Zheng, Z. Bie, Y. Sun, J. Wang, C. Su, S. Wang, and Q. Tian. Mars: A video benchmark for large-scale person re-identification. In *European Conference on Computer Vision*, pages 868–884. Springer, 2016. [3](#), [5](#)

[45] L. Zheng, L. Shen, L. Tian, S. Wang, J. Wang, and Q. Tian. Scalable person re-identification: A benchmark. In *Proceedings of the IEEE International Conference on Computer Vision*, pages 1116–1124, 2015. [1](#), [2](#), [3](#), [5](#), [6](#), [7](#)

[46] L. Zheng, Y. Yang, and A. G. Hauptmann. Person re-identification: Past, present and future. *arXiv preprint arXiv:1610.02984*, 2016. [1](#), [3](#), [5](#), [6](#), [7](#)

[47] L. Zheng, Y. Yang, and Q. Tian. Sift meets cnn: a decade survey of instance retrieval. *arXiv preprint arXiv:1608.01807*, 2016. [1](#)

[48] L. Zheng, H. Zhang, S. Sun, M. Chandraker, and Q. Tian. Person re-identification in the wild. *arXiv preprint arXiv:1604.02531*, 2016. [2](#), [3](#), [5](#)

[49] Z. Zheng, L. Zheng, and Y. Yang. A discriminatively learned cnn embedding for person re-identification. *arXiv preprint arXiv:1611.05666*, 2016. [3](#), [6](#), [7](#)